Reprinted from:
THE JOURNAL OF CHEMICAL PHYSICS VOLUME 56, NUMBER 7 1 APRIL 1972

Effect of Pressure on the Electronic Structure of Twelve Ferric β-Diketone Complexes*

C. W. Frank and H. G. Drickamer
School of Chemical Sciences and Materials Research Laboratory, University of Illinois, Urbana, Illinois 61801

(Received 22 November 1971)

The effect of pressure to 180 kbars on the electronic structure of 12 ferric β-diketone complexes has been measured by means of Mössbauer resonance and optical absorption. The systematic variation of the electron donor and acceptor properties of the ligands permits a more detailed interpretation of the results than in previous studies. These properties are correlated with the isomer shift of the Fe(III), and that of the Fe(II) produced under pressure, and with the change of the isomer shifts with pressure. The degree of conversion of Fe(III) to Fe(II) correlates well with the change of isomer shift with pressure, and thus with changes of the electronic properties of the ligands. Optical absorption studies as a function of pressure were made on both the charge transfer and intraligand $\pi\rightarrow\pi^*$ transitions of several complexes. The decrease in area under the CT peaks correlates very well with the amount of reduction of Fe(III) as obtained from the Mössbauer resonance studies. The shifts of both the CT peaks and $\pi\rightarrow\pi^*$ transitions are recorded and discussed briefly.

In this paper, we discuss the effect of pressure to 180 kbars on the electronic state of iron in a series of complexes with β-diketones. The experimental techniques used were Mössbauer resonance and optical absorption. These have been described previously.[1–3]

A series of studies since 1967 has revealed changes of both spin state and oxidation state of iron with increasing pressure.[4–9] Ferric iron tends to reduce to the ferrous state; for ferrous iron one observes either conversion from high spin to low spin or from low spin to high spin with pressure for various materials in different pressure ranges.

While the reduction of ferric iron has been observed in a wide variety of compounds, there has been no study where the electron donor properties of the ligand have been varied in a systematic way, nor have the Mössbauer resonance studies generally been accompanied by appropriate optical absorption measurements. We present such a systematic study here.

The previous measurements of the reduction of Fe(III) at high pressure have, however, revealed a number of general characteristics. The reduction takes place over a range of pressure, and does not go to completion within the limits of available pressure, at least at 25°C. Over a considerable range of pressure the conversion can frequently be approximated by the expression

$$K=C_{\mathrm{II}}/C_{\mathrm{III}}=AP^M,$$

where C_{II} and C_{III} are the fractions of ferrous and ferric sites; P is the pressure; and A and M are constants. The process is endothermic. It is reversible, but with considerable hysteresis. These characteristics are accounted for in a thermodynamic analysis presented by Slichter and Drickamer[10] which is analogous to a molecular field theory of magnetism or to the regular solution theory of nonideal mixtures.

From an electronic viewpoint, the process involves transfer of an electron from nonbonding or weakly bonding ligand orbitals to the nonbonding or slightly antibonding metal $d_\pi(t_{2g})$ orbitals. A number of observations are consistent with a decrease in the energy difference between the ligand π and metal d_π orbitals. The interelectronic repulsion (Racah) parameters generally decrease with increasing pressure. This is associated with a spreading of the $3d$ orbitals due to increasing central field covalency. The fact that the isomer shift (center of the Mössbauer spectrum measured with respect to *bcc* iron) decreases with pressure indicates that there is a higher electron density at the iron nucleus because of the decreased shielding of the $3s$ orbital by the $3d$ electrons. It is very difficult to find optical absorption peaks which are unequivocally assigned to the $\pi\rightarrow t_{2g}$ transition. However, peaks with substantial charge transfer character shift to lower energy and broaden with increasing pressure. These peaks typically lie in the range 2–4 eV and shift by several tenths of an electron volt in 100 kbars.

A large difference between optical and thermal transition energies is not unusual. Color centers, which have absorption peaks in the range 2–4 eV, can be bleached thermally at moderate temperatures, sometimes as low as 100°K. Redox reactions in solution, where the thermal energy difference between states is essentially zero, absorb in the visible region of the spectrum. Analyses by Marcus[11,12] and by Hush[13,14] can be modified to indicate a first approximation to the difference in thermal energy between initial and final states at 25°C:

$$E_{\mathrm{th}}=h\nu_{\max}-3.6(\Delta\nu_{1/2})^2(\omega/\omega')^2,$$

where $\nu_{\max}$ is the optical absorption maximum, $\Delta\nu_{1/2}$ is the halfwidth of the charge transfer peak in eV, and ω and ω' are the force constants for the ground and excited state potential wells. Both the observed red shift and broadening thus contribute to the change of ground state with pressure.

There are a number of factors which make the difference between thermal and optical energies reasonable. In the first place, the Franck–Condon principle requires optical transitions to occur vertically on a configuration coordinate diagram, while thermal processes are not so restricted. In the second place, the optical processes are subject to selection rules, while

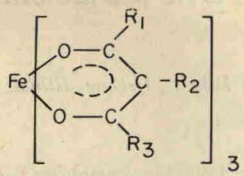

LIGAND	R_1	R_2	R_3
1. ACA	$-CH_3$	-H	$-CH_3$
2. DBM		-H	
3. DPM	$-C(CH_3)_3$	-H	$-C(CH_3)_3$
4. BA		-H	$-CH_3$
5. TFACA	$-CF_3$	-H	$-CH_3$
6. FTFA	$-CF_3$	-H	
7. TTFA	$-CF_3$	-H	
8. BTFA	$-CF_3$	-H	
9. MACA	$-CH_3$	$-CH_3$	$-CH_3$
10. PACA	$-CH_3$		$-CH_3$
11. NACA	$-CH_3$	$-NO_2$	$-CH_3$
12. EACA	$-CH_3$	$-C_2H_5$	$-CH_3$

FIG. 1. Compounds studied.

the thermal processes occur over sufficient time that their selection rules are relaxed. In the third place, there will almost certainly be strong configuration interaction in the solid state which can increase the difference between thermal and optical energy requirements. Finally, the pressure selects the volume as a configuration coordinate,whereas optical processes may involve other configuration coordinates; this may further increase the energy difference for the two processes.

The reduction process has thus been characterized and justified in a general way. To relate the reduction in a systematic way to the electron donor characteristics of the ligand, we have studied the 12 β-diketone complexes shown in Fig. 1.

All except one of the derivatives were prepared by the ferric acetate procedure as described by Hantzsch and Desch,[15] with some modifications. In order to obtain satisfactory Mössbauer spectra it was necessary to use ^{57}Fe enriched iron in the syntheses of the compounds. The enriched iron used in these preparations was purchased from Oak Ridge National Laboratory, Oak Ridge, Tennessee, in the form of α-Fe_2O_3 containing 77% ^{57}Fe. Metallic iron was prepared by reducing the α-Fe_2O_3 at 480°C in a hydrogen atmosphere over a period of 3 hrs. Each synthesis of an enriched compound was done on a microscale, yielding approximately 20 mg of product.

For each enriched synthesis, the iron powder was dissolved in 0.4*N* HCl and then oxidized with chlorine gas to give a yellow solution. Molecular chlorine was removed by purging with a nitrogen stream and the *p*H was adjusted to about 5 by means of solid sodium acetate. An ethanolic solution of the β-diketone ligand, 20% in excess, was then added to the iron solution. Generally 2 ml of ethanol were mixed with the liquid β-diketones; considerably more was required for the solid ligands. Usually the chelate precipitated immediately. In some cases, however, it was necessary to let the solution sit in a refrigerator for three or four hours. The precipitate was then washed with water or a 50–50 ethanol–water solution and dried under vacuum.

Generally the chelates were prepared with commercially available substituted β-diketones. Since the nitro substituted ligand could not be so obtained, the procedure of Sen and Thankarajan[16] was used to nitrate ferric acetylacetonate. In all cases the synthesis procedure was first checked using unenriched iron. The enriched material was prepared only after a satisfactory microanalysis had been obtained.

The samples prepared for optical work were made in considerably larger quantities. Here is proved simpler first to dissolve $FeCl_3$ in water and remove the undissolved material by filtration. The remainder of the procedure was identical.

DISCUSSION

In the following sections we discuss first the Mössbauer resonance results, the interpretation of the change of isomer shift with pressure, and then the conversion of ferric to ferrous iron with pressure. The second section discusses the optical absorption measurements, the assignment of the peaks in the visible and uv, the change in area under the charge transfer peaks with pressure, and, briefly, the shift of the peak locations with pressure.

Mössbauer Resonance

A minimum of two complete pressure runs was made on each compound. The samples were diluted at least 8/1 with boron to eliminate any effect of sample thickness. Considerable care was taken in the loading procedure to minimize shear. Typical Mössbauer spectra are shown in Figs. 2(a) and 2(b). The data were fit to Lorentzian peaks using a least squares fitting program. The locations of these peaks give the isomer shifts (presented here with respect to metallic iron) and the quadrupole splittings.

The relative areas under the ferrous and ferric peaks give the relative conversion. (It is necessary to assume equal *f* number at ferrous and ferric sites.) Fits at low pressure were particularly difficult because of the low peak intensity and the asymmetric nature of the ferric peaks due to spin–spin coupling.[17] It can be seen from Fig. 2 that conversion increases continuously with pressure. After release of pressure and some effort to re-

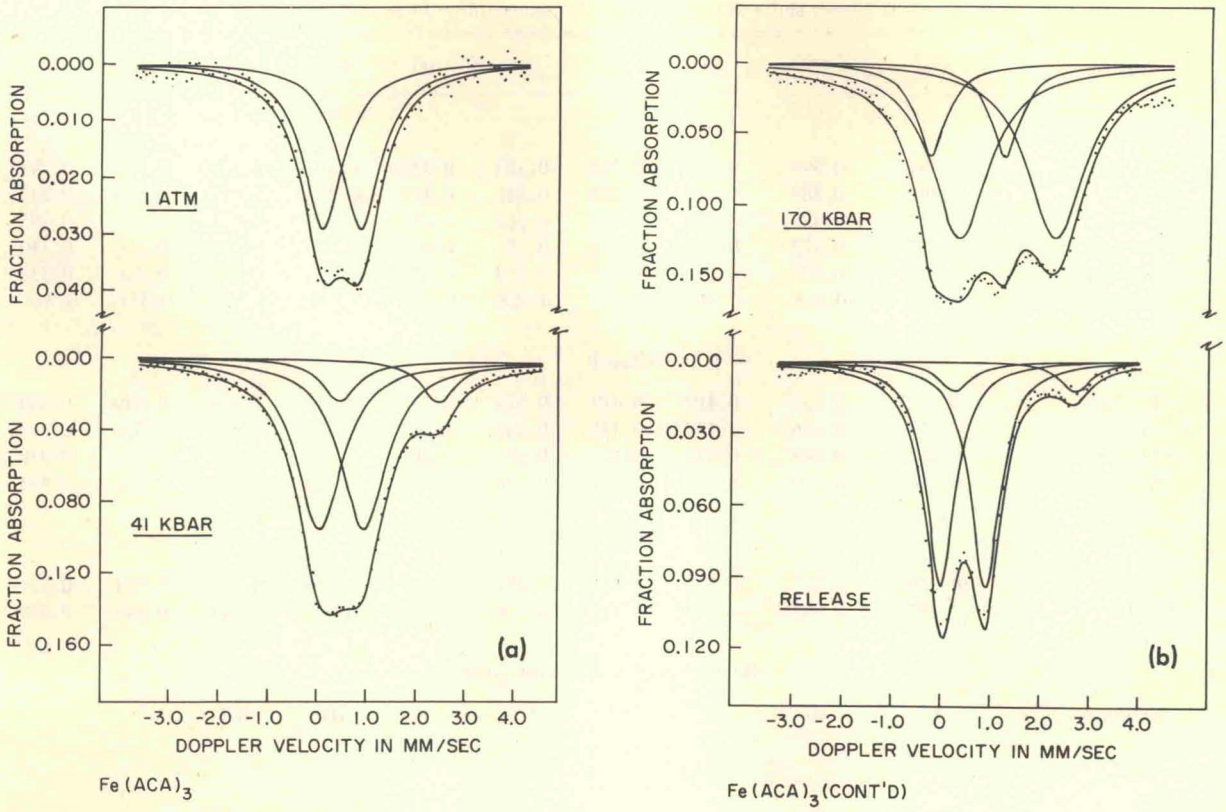

FIG. 2. (a) Mössbauer spectra for ACA(1). (b) Mössbauer spectra for ACA(1) (cont'd.).

move strain by powdering the sample, the spectrum returns substantially to the ferric state (see lower part of Fig. 2b). The strain removal process is inefficient with such a small sample; we feel that complete release of strain would probably give an entirely ferric spectrum. In Figs. 3 and 4 are plotted the raw data for the ferrous and ferric isomer shifts for ACA(1) to give some idea of the scatter. Smoothed values for isomer shifts and quadrupole splittings appear in Tables I and II. The classification of compounds is discussed a little later in the paper.

Isomer Shifts

In analyzing the factors influencing the degree of conversion of Fe(III) to Fe(II) with pressure, it is desirable to have a measure of the tendency of the ligand to donate or withdraw electrons at high pressure. There are a number of possible measures of this tendency at one atmosphere, which, as we shall show, correlate well with the ferric isomer shift.

One measure of the electronic character of the β-diketone is the acid dissociation constant associated with the enol form in the keto–enol equilibrium. Substituent effects are analyzed in terms of the tendency

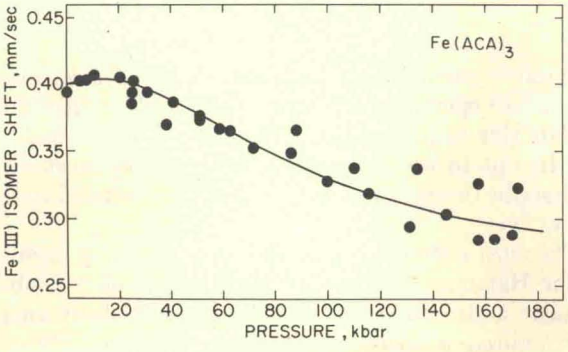

FIG. 3. Fe(III) isomer shift vs pressure—ACA(1).

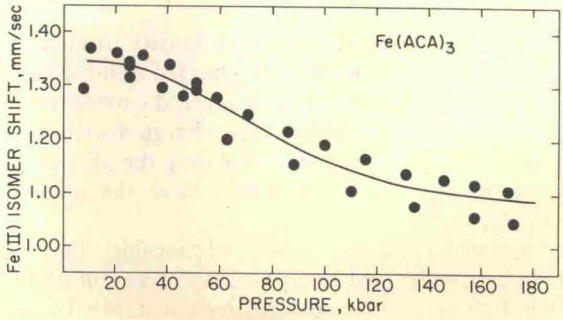

FIG. 4. Fe(II) isomer shift vs pressure—ACA(1).

TABLE I. Isomer shifts vs pressure Fe(III) isomer shift.[a] Pressure (kbar).

Derivative	Atm	20	40	60	80	100	120	140	160	180
					Class A					
ACA(1)	0.394	0.399	0.385	0.368	0.350	0.335	0.322	0.309	0.299	0.294
BA(4)	0.390	0.389	0.385	0.372	0.347	0.314	0.288	0.267	0.253	0.243
TFACA(5)	0.458	0.420	0.396	0.379	0.362	0.345	0.330	0.316	0.305	0.295
MACA(9)	0.357	0.372	0.374	0.365	0.353	0.343	0.333	0.325	0.316	0.310
NACA(11)	0.429	0.423	0.413	0.402	0.389	0.376	0.366	0.355	0.346	0.336
EACA(12)	0.362	0.358	0.345	0.335	0.328	0.322	0.318	0.315	0.314	0.313
					Class B					
FTFA(6)	0.450	0.430	0.419	0.419	0.425	0.437	0.446	0.448	0.449	0.449
TTFA(7)	0.455	0.436	0.424	0.416	0.409	0.404	0.400	0.397	0.394	0.390
BTFA(8)	0.462	0.444	0.427	0.410	0.398	0.390	0.384	0.381	0.380	0.379
PACA(10)	0.370	0.419	0.435	0.437	0.436	0.432	0.428	0.423	0.417	0.413
					Class C					
DBM(2)	(0.250)	(0.315)	0.376	0.439	0.481	0.505	0.516	0.521	0.524	0.524
DPM(3)	(0.250)	0.328	0.400	0.441	0.478	0.508	0.529	0.544	0.549	0.550

Fe(II) Isomer shift. Pressure (kbar).

Derivative	40	60	80	100	120	140	160	180
				Class A				
ACA(1)	1.320	1.267	1.213	1.171	1.141	1.116	1.095	1.081
BA(4)	1.290	1.215	1.159	1.119	1.088	1.066	1.052	1.042
TFACA(5)	1.290	1.239	1.199	1.171	1.150	1.132	1.115	1.098
MACA(9)	1.276	1.269	1.227	1.178	1.141	1.120	1.111	1.106
NACA(11)	1.260	1.226	1.200	1.177	1.158	1.148	1.143	1.140
EACA(12)	1.286	1.249	1.213	1.181	1.157	1.141	1.131	1.125
				Class B				
FTFA(6)	1.135	1.084	1.065	1.063	1.063	1.063	1.063	1.063
TTFA(7)	(1.10)	1.069	1.046	1.027	1.015	1.006	1.001	0.996
BTFA(8)	1.100	1.074	1.058	1.049	1.044	1.041	1.040	1.039
PACA(10)	1.066	1.059	1.051	1.046	1.041	1.038	1.034	1.030
				Class C				
DBM(2)	1.095	1.014	0.991	0.989	0.989	0.989	0.989	0.989
DPM(3)	1.171	1.150	1.128	1.108	1.089	1.074	1.060	1.050

[a] Relative to *bcc* iron, mm/sec.

to increase or reduce the electron density around the oxygen atoms in the negatively charged anionic form. Electron donating groups will increase the oxygen electron density and destabilize the charge distribution, thus lowering the acidity and increasing the pK_D value. Electron withdrawing groups will have the opposite effect.

A second semiquantitative relationship between chemical structure and electron donor–acceptor ability is given by electrophilic substitution constants. In general such correlations have been applied mainly to aromatic systems where both inductive and resonance effects are operative. However, to the extent that the chelate ring is quasiaromatic in nature, it is reasonable to attempt to use electrophilic substitution constants to describe the electronic properties of the metal chelate derivatives.

The most common method of doing this is by means of the Hammett σ, which is characteristic of the substituent added to the parent structure. Substituents with positive σ values are stronger electron acceptors than hydrogen; negative values indicate a weaker tend-

TABLE II. Quadrupole splitting vs pressure Fe(III) quadrupole splitting.[a] Pressure (kbar).

Derivative		20	40	60	80	100	120	140	160	180
					Class A					
ACA(1)	S[b]	0.775	0.896	1.049	1.191	1.308	1.396	1.458	1.503	1.534
BA(4)	A	0.771	0.957	1.172	1.347	1.469	1.558	1.612	1.649	1.662
TFACA(5)	A	0.675	0.827	0.982	1.156	1.340	1.483	1.562	1.593	1.605
MACA(9)	S	0.820	0.923	1.030	1.136	1.231	1.314	1.378	1.409	1.420
NACA(11)	S	0.825	0.944	1.082	1.238	1.397	1.509	1.558	1.579	1.591
EACA(12)	S	0.921	1.056	1.172	1.276	1.358	1.419	1.460	1.480	1.488
					Class B					
FTFA(6)	A		0.822	0.948	1.169	1.408	1.600	1.714	1.761	1.775
TTFA(7)	A	0.781	0.943	1.110	1.279	1.446	1.591	1.697	1.741	1.750
BTFA(8)	A		0.873	1.109	1.330	1.521	1.671	1.776	1.832	1.845
PACA(10)	S	0.660	0.872	1.033	1.150	1.250	1.329	1.378	1.400	1.409
					Class C					
DBM(2)	S		0.921	1.022	1.174	1.370	1.538	1.619	1.649	1.660
DPM(3)	S		0.721	0.939	1.158	1.319	1.411	1.447	1.453	1.453

Fe(II) Quadrupole splitting. Pressure (kbar).

Derivative	40	60	80	100	120	140	160	180
			Class A					
ACA(1)	2.002	1.954	1.926	1.916	1.922	1.934	1.942	1.945
BA(4)	2.050	1.977	1.935	1.916	1.916	1.929	1.946	1.966
TFACA(5)	2.248	2.123	2.055	2.046	2.068	2.094	2.115	2.122
MACA(9)	2.180	2.180	2.180	2.189	2.206	2.220	2.224	2.224
NACA(11)	2.081	2.147	2.202	2.248	2.289	2.321	2.338	2.342
EACA(12)	2.275	2.191	2.148	2.129	2.122	2.120	2.120	2.120
			Class B					
FTFA(6)	2.225	2.132	2.095	2.102	2.130	2.144	2.148	2.149
TTFA(7)		1.982	1.990	2.017	2.044	2.060	2.065	2.065
BTFA(8)	2.365	2.175	2.040	2.003	2.018	2.051	2.075	2.082
PACA(10)	2.305	2.215	2.148	2.107	2.088	2.080	2.074	2.070
			Class C					
DBM(2)	2.190	2.078	2.028	2.015	2.014	2.014	2.014	2.014
DPM(3)	2.486	2.447	2.412	2.384	2.375	2.395	2.418	2.423

[a] In mm/sec. [b] *S*-symmetric substitution, *A*-asymmetric substitution.

ency for electron attraction than hydrogen. The σ values reflect a combination of inductive and resonance effects and are sensitive to the position of substitution. Brown and Okamoto[18] have shown that better correlations can be obtained for electrophilic reactions using slightly modified σ values. Both sets of substituent values work equally well for the compounds, so the σ^+ set has been used here.

The third chemical parameter which can be related to the electronic behavior of the ligand derivatives is the appearance potential from electron impact mass spectrometry. The technique involves bombarding the substance in the gas phase with electrons and monitoring the ion current produced as the range of accelerating voltages is scanned. The appearance potential of interest in the metal β-diketonate systems corresponds to that voltage at which the singly ionized ML_3^+ species appears. Here M refers to the metal and L to the ligand.

Numerous examinations of the β-diketonate derivatives of the first transition series metals[19–24] have indicated that the appearance potentials depend predominantly on the ligand and only slightly on the metal.

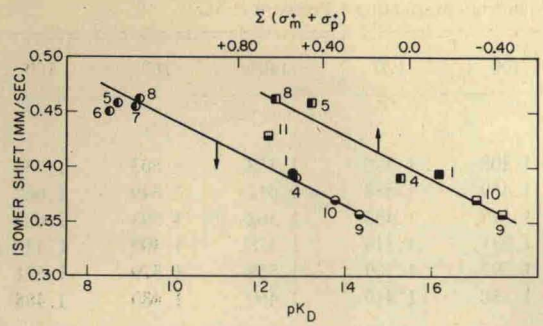

FIG. 5. Fe(III) isomer shift vs pk_D and Hammett σ.

Thus, data for the homologous series of Cu(II) chelates have been used because data for the Fe(III) chelates were incomplete.

Still another chemical parameter from which electronic information may be deduced is the half wave potential $E_{1/2}$ from polarography. Electron donating groups on the chelate ring will tend to increase the basicity of the oxygen atoms and impart strong covalent character to the metal–oxygen bond. This will result in a large negative value of the half-wave potential. Withdrawing groups lead to more ionic metal–oxygen bonds and a less stable chelate with a less negative half wave potential. As was previously the case, no literature data were available for the iron series derivatives. However, several investigations of the copper series[25–29] have been made and are used here.

Variations in the order of electron donor ability among the derivatives, as predicted by these different chemical correlations, do exist. However, three rough groupings of compounds are readily apparent. These are, in decreasing order of electron donor ability: [DPM(3), MACA(9), PACA(10), EACA(12)]> [ACA(1), DBM(2), BA(4)]>[TFACA(5), FTFA(6), TTFA(7), BTFA(8), NACA(11)] where the members of each general group have been arbitrarily arranged in order of their reference code.

Figures 5 and 6 show the correlation between atmospheric Fe(III) isomer shifts determined in this work, and the various atmospheric chemical measurements obtained from the literature. The isomer shift is given relative to *bcc* iron and the chemical parameters have been plotted so that movement to the right corresponds to an increase in electron donor tendency. The numbers refer to the reference codes given in Fig. 1. The same general correlation is observed in all cases, i.e., the smaller isomer shift, or greater s electron density at the iron nucleus, may be associated with a greater tendency for donation of the ligand electrons to the metal. It is important to realize, however, that the absolute value of the isomer shift depends on several contributions, as has been pointed out by Erickson.[30] The isomer shift is affected by metal orbital expansion

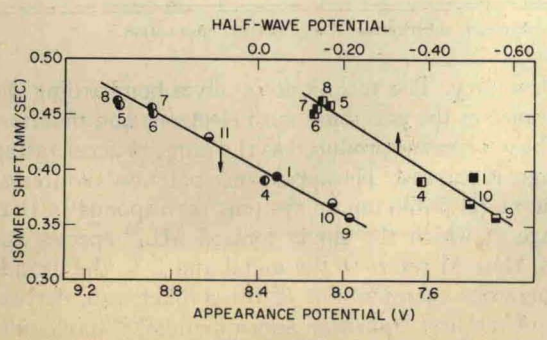

FIG. 6. Fe(III) isomer shift vs half wave potential and appearance potential.

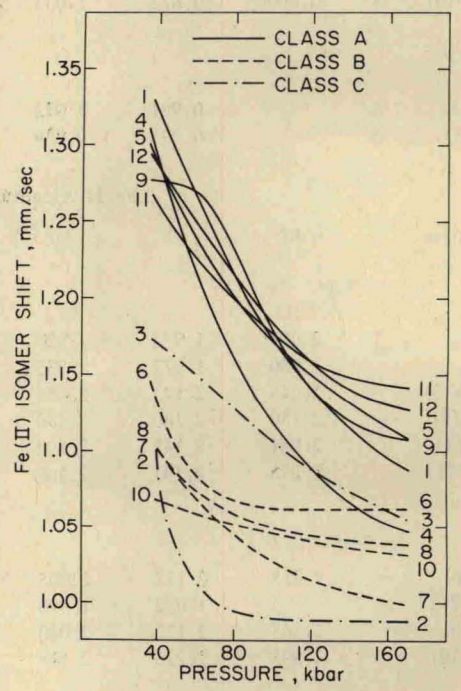

FIG. 7. Fe(II) isomer shifts vs pressure.

due to a reduction of effective nuclear charge associated with the overlap of the metal electron cloud with the negative ligand charge, and by 4s orbital augmentation, which constitute central field covalency. In addition, metal d_π backbonding to vacant ligand π^* orbitals or 3s shielding because of overlap of ligand electron density in the bond region, which constitute symmetry restricted covalency, are important factors to consider. Since these contributions may well exhibit different pressure behavior, the fact that the correlations of isomer shifts and measures of electron donor tendencies at atmospheric pressure are fairly consistent does not necessarily imply that such a correlation of absolute isomer shifts with degrees of conversion will be as good at high pressures.

It is convenient to group the derivatives studied into smaller classes (A, B, and C) so that the pressure behavior may be discussed. These classifications are based on the isomer shift behavior of both oxidation states as a function of pressure above 40–50 kbars. They are not rigid, e.g., at low pressures PACA(10) is more like a Class A compound and at high pressures FTFA(6) approaches Class C behavior.

Similarities in behavior of the Fe(II) isomer shifts which lead to classifications will be considered first, followed by an examination of the consistencies in the Fe(III) isomer shifts.

Some interesting observations may be made if the smoothed data for all the derivatives are plotted on a single figure as shown in Fig. 7. The six derivatives drawn with solid curves, ACA(1), BA(4), TFACA(5), MACA(9), NACA(11), and EACA(12) will be referred to as Class A. These are closely grouped at low pressures with Fe(II) isomer shifts in the range 1.26–1.32 mm/sec, typical of systems with little or no metal-to-ligand backdonation.

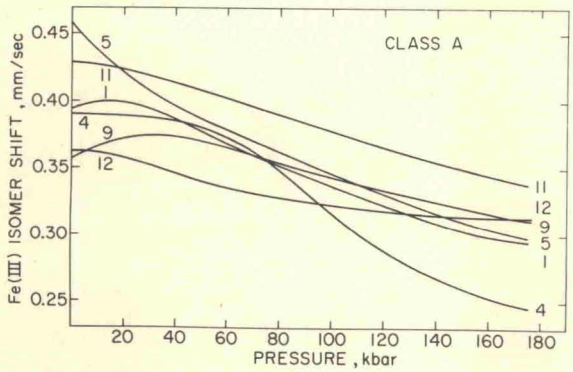

FIG. 8. Fe(III) isomer shifts vs pressure—Class A.

On the basis of Fe(II) isomer shift data, the members of the second class are FTFA(6), TTFA(7), BTFA(8), and PACA(10). The Class B derivatives have distinctly smaller low pressure Fe(II) isomer shifts (1.06–1.14 mm/sec) than the members of Class A. Such values indicate a considerably larger backdonation. However, the decrease of Fe(II) isomer shifts with pressure is not nearly as large as Class A; the final values lie between 0.99–1.06 mm/sec. This is due to a reduction in backdonation as explained in the following section on Fe(III) isomer shifts. Fe(III) isomer shift data for FTFA(6) and PACA(10) are somewhat atypical for this group. The former exhibits properties similar to Class C at high pressure and the latter to Class A at low pressure. Nevertheless, this grouping will be retained for purpose of discussion.

The final grouping of DBM(2) and DPM(3) in Class C appears somewhat arbitrary on the basis of Fe(II) isomer shift data. However, the classification may be rationalized on the basis of Fe(III) isomer

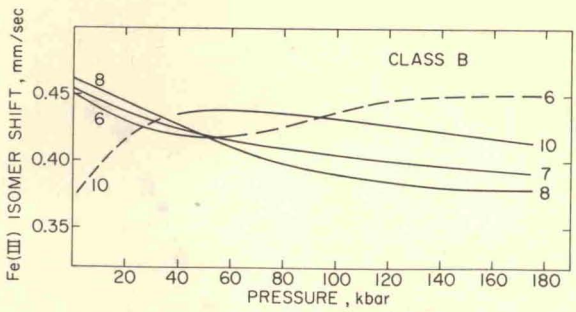

FIG. 9. Fe(III) isomer shifts vs pressure—Class B.

shifts. Although both DBM(2) and DPM(3) show lower Fe(II) isomer shifts than members of Class A, their smoothed values completely bracket those of Class B. The very low Fe(II) isomer shift of DBM(2) indicates rather extensive backdonation to the aromatic terminal substituents. Certainly the tertiary butyl groups in DPM(3) would not allow for as much delocalization.

The pressure behavior of Fe(III) isomer shifts can now be considered in terms of consistencies with and deviations from the classification which has been presented. The smoothed values for all of the derivatives are arranged by classes in Figs. 8, 9, and 10. The ability of the Fe(III) isomer shift to reflect the electron donor tendencies of the surrounding ligands, at least in the low pressure region, has already been noted. Thus it is reasonable that for Class A the electron donating methyl [MACA(9)] and ethyl [EACA(12)] derivatives should have low isomer shifts and that the electron withdrawing trifluoromethyl [TFACA(5)] and nitro [NACA(11)] derivatives have high isomer shifts, with ACA(1) and BA(4) intermediate. Because of the fairly broad range of properties, the atmospheric isomer shifts cover a rather large range, from 0.36–0.46 mm/sec. The typical behavior of the ferric isomer shift, as observed in many other compounds, is to decrease with pressure because of an expansion of the *d* orbitals and subsequent reduction of shielding of the 3*s* orbital. Evidence for such metal orbital expansion

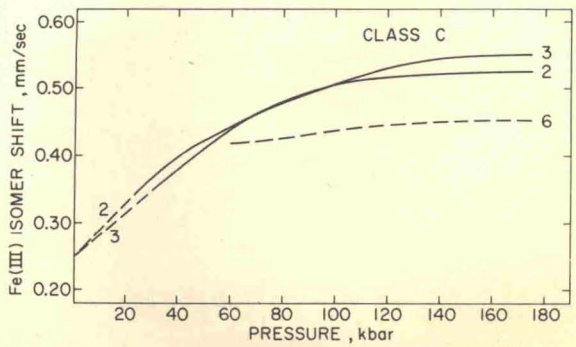

FIG. 10. Fe(III) isomer shifts vs pressure—Class C.

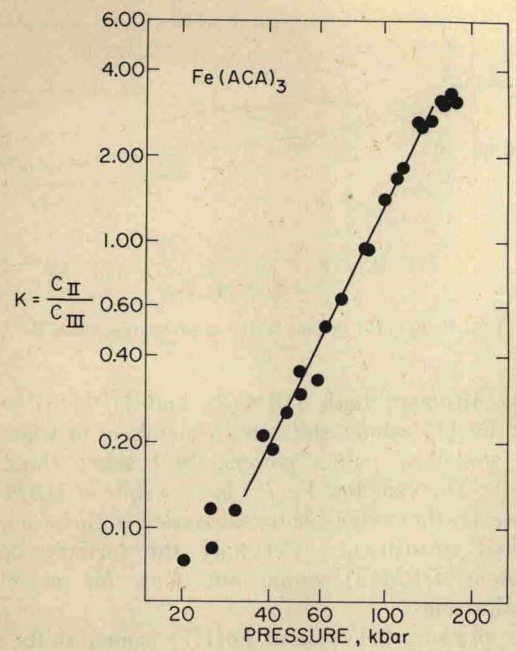

FIG. 11. Log K vs log P—ACA(1).

is provided by measurements of the Racah parameter B in other transition metal chelates in which decreases of 5%–10% in 100 kbars were obtained.[31,32] The isomer shifts for the Class A compounds do show net decreases over the pressure range but in the low pressure region, except for TFACA(5), they exhibit very small decreases or even increases and subsequent maxima at moderate pressures. This behavior may be explained

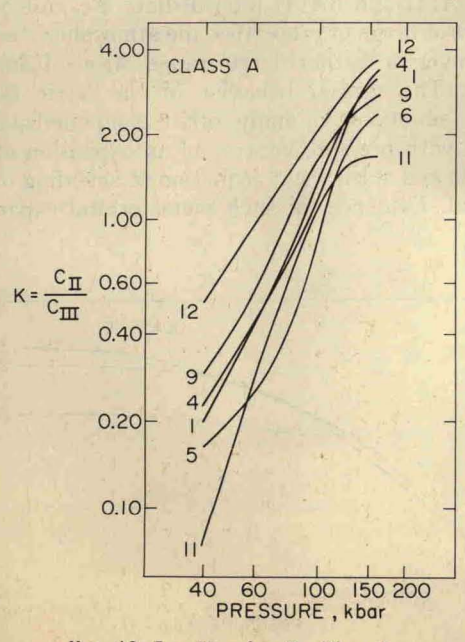

FIG. 12. Log K vs log P—Class A.

in terms of competition among the various contributions to the isomer shift. It is presumed that all of the derivatives have some 4s occupation in the ferric state, the extent varying from compound to compound. The inductive effects exhibited by the various substituents through the σ bonding system should be important in this respect, with good σ donors such as the alkyl groups increasing the 4s augmentation and poor σ donors such as the trifluoromethyl group decreasing it. With pressure the 4s orbital, which is σ antibonding, will increase in energy with respect to the metal 3d and ligand π and π^* orbitals due to increased overlap with ligand σ orbitals. This will cause a decrease of 4s occupation and an increase in isomer shift which of course is counter to the result expected from a delocalization of the metal d electrons. Thus a competitive balance will be maintained for each compound and

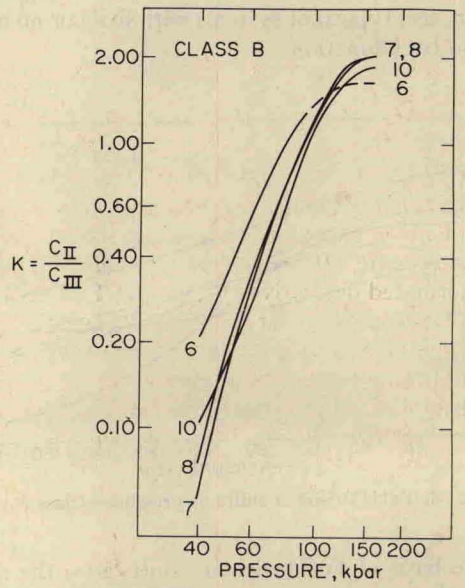

FIG. 13. Log K vs log P—Class B.

the possibility of maxima in the isomer shift curves is apparent.

In contrast to the other derivatives of Class A, TFACA(5), a strong σ acceptor with the highest initial isomer shift, shows a very large initial decrease in IS. This may be attributed to a very low initial 4s occupation so that the spreading of the d orbitals is the predominant pressure effect. The initial differences in behavior among the members of Class A are reduced above 100 kbars as the smoothed curves for four of the derivatives [ACA(1), TFACA(5), MACA(9), and EACA(12)] form a narrow band of about 0.02 mm/sec width with NACA(11) lying about 0.03 mm/sec above and BA(4) from 0.03–0.05 mm/sec below. In its shift behavior, BA(4) shows quite a large decrease with pressure and is again lower than the other members

TABLE III. Percent conversion to Fe(II). Pressure (kbar).

Derivative	40	60	80	100	120	140	160	180[a]
				Class A				
ACA(1)	16.4	29.7	44.3	57.9	67.7	73.3	75.7	76.4
BA(4)	18.3	30.1	42.2	54.0	65.3	73.5	77.1	77.5
TFACA(5)	13.8	20.8	29.6	45.5	60.4	67.6	70.0	70.5
MACA(9)	20.3	35.6	51.1	62.2	67.9	71.1	73.1	74.5
NACA(11)	7.1	21.7	38.2	52.0	59.2	61.8	62.4	62.4
EACA(12)	34.0	48.9	59.3	67.0	72.8	76.6	78.5	78.8
				Class B				
FTFA(6)	17.0	35.0	50.4	58.3	61.4	62.0	62.0	62.0
TTFA(7)	5.3	23.6	41.4	55.3	63.8	66.5	67.0	67.0
BTFA(8)	7.0	25.2	41.6	54.4	62.5	66.2	67.0	67.0
PACA(10)	9.4	21.1	37.4	53.2	60.5	64.2	65.0	65.0
				Class C				
DBM(2)	25.2	42.5	52.0	55.6	56.7	57.0	57.0	57.0
DPM(3)	39.0	48.6	55.8	60.5	63.8	66.0	67.2	67.5

[a] Extrapolated values.

of Class A at higher pressures. This is analogous to the behavior of its Fe(II) isomer shift.

The smoothed curves for Class B are shown in Fig. 9. The atmospheric and low pressure behavior of the three fluorinated derivatives FTFA(6), TTFA(7), and BTFA(8) are very similar, with the fairly high values (0.45–0.46 mm/sec) predominantly due to the presence of the electronegative trifluoromethyl group. There is no tendency toward maxima in the low pressure region for these three derivatives. This is consistent with the assumption that the trifluoromethyl group reduces the initial 4*s* augmentation to very small values. However, in contrast to the large TFACA(5) isomer shift decrease of 0.16 mm/sec over the whole pressure range, TTFA(7) and BTFA(8) show much smaller decreases of 0.07 and 0.08 mm/sec, respectively. FTFA(6) shows an increase at higher pressures. The similar behavior of TTFA(7) and BTFA(8) is reasonable on the basis of the structure of the second terminal substituent, where the sulfur in the heterocyclic thiophene ring of TTFA(7) has the same Pauling electronegativity as carbon in the phenyl ring of BTFA(8). The fourth member of the class, PACA(10), also exhibits only a rather small decrease in isomer shift above 50 kbars.

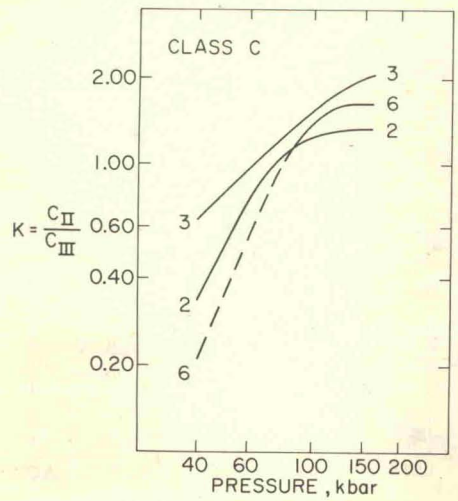

FIG. 14. Log K vs log P—Class C.

It has been already noted that, on the basis of Fe(II) isomer shifts, these derivatives show extensive backbonding in the ferrous state. Backbonding would be expected for the ferric state also but in general this state has less than the ferrous state. The relatively small decreases in isomer shift may then be associated with a decrease in backbonding with pressure such as that observed in phenanthroline complexes and some ferrocyanides.[5,9,33]

PACA(10) shows typical Class B behavior above 50 kbars with a rather slight decrease in Fe(III) isomer shift. However, it is distinguished by the very large increase in isomer shift in the low pressure region. Such an increase is similar in form, if not in degree, to those observed in several Class A derivatives. The 4*s* augmentation argument should apply but it seems unlikely to be the only effect as the increase is so large. The answer may lie in one of the contributions of symmetry restricted covalency to the isomer shift, e.g., involving overlap of ligand electron density in the metal bond region. If the ligand overlap should extend inside the 3*s* orbital, the isomer shift will increase due

TABLE IV. Equilibrium constant parameters.

Derivative	A	M	Pressure range
	Class A		
ACA(1)	5.82×10^{-5}	2.18	40–150
BA(4)	5.30×10^{-5}	2.19	55–165
TFACA(5)	2.18×10^{-6}	2.80	65–140
MACA(9)	2.06×10^{-4}	1.94	40–120
NACA(11)	2.46×10^{-6}	2.83	40–110
EACA(12)	1.88×10^{-3}	1.52	40–150
	Class B		
FTFA(6)	2.69×10^{-5}	2.42	40–85
TTFA(7)	3.61×10^{-6}	2.76	50–120
BTFA(8)	5.91×10^{-6}	2.65	50–115
PACA(10)	3.09×10^{-6}	2.78	45–115
	Class C		
DBM(2)	2.64×10^{-4}	1.94	40–75
DPM(3)	1.70×10^{-2}	0.98	40–120

to the resulting shielding of the 3s. Of course one would expect pressure to increase such overlap generally for all the derivatives but the effect may not be important unless there is appreciable initial steric hindrance. There is ample evidence that the phenyl ring in PACA(10) is not coplanar with the chelate ring as a result of steric inhibition. Thus it seems possible that the additional crowding would lead to greater ligand overlap and hence an increase in isomer shift.

The Fe(III) isomer shifts for Class C, consisting of DBM(2) and DPM(3), are shown in Fig. 10. Low pressure data are difficult to obtain because of the very low percent effect and the non-Lorentzian broadening referred to earlier. (This broadening diminishes with increasing pressure and becomes insignificant above 70 kbars.) However, it appears that both isomer shifts are rather low, in the region of 0.25 mm/sec. The low values probably arise from different effects with extensive d_π delocalization to the two aromatic rings predominating in DBM(2) and appreciable σ donation from the tertiary butyl groups in DPM(3). The important feature is that both derivatives show quite large increases in Fe(III) isomer shift so that at the highest pressure the values range between 0.52–0.55 mm/sec. As already mentioned, FTFA(6) also shows an increase in isomer shift in the high pressure region qualitatively similar to DBM(2) and DPM(3). The increase in isomer shift may be explained in part by the reduction of backbonding and 4s occupation with pressure for DBM(2) and DPM(3), respectively. In addition, there are probably contributions due to 3s shielding arising from overlap with occupied ligand orbitals.

Reduction of Fe(III) *to* Fe(II)

We turn now to a discussion of the reduction of Fe(III) to Fe(II). The general characteristics of this process have been presented earlier. We emphasize here the correlation with electronic properties. Typical conversion data in the form of log$K$ are plotted as a function of log$P$ for ACA(1) in Fig. 11. The linear plot holds over a considerable pressure range. The deviations at low pressure may be associated with difficulties in measuring conversions below 10%. High pressure deviations are discussed below.

Smoothed conversion data for Classes A, B, and C are shown in terms of equilibrium constant plots in Figs. 12, 13, and 14 with the tabulated conversions given in Table III. The constants A and M in the empirical relation for the equilibrium constant $K=AP^M$ are given in Table IV. The conversion behavior of the three classes provides further justification for the classification scheme. For example, Class A derivatives show continuously increasing conversion over the whole pressure range. Furthermore, the linear behavior is obtained over a substantial portion of the range, with an upper limit between 140–165 kbars for ACA(1), BA(4), TFACA(5), and EACA(12). MACA(9) appears to show a change of slope at about 110 kbars but increases steadily thereafter. On the other hand, NACA(11) tends to level off at high pressures.

Class B derivatives show linear behavior between roughly 45–115 kbars and show distinct tendencies to level off and become independent of pressure above 150 kbars. The only exception to this behavior is shown by FTFA(6) which appears to exhibit Class B properties in the low pressure region but Class C behavior at high pressure. The slopes of the conversion curves in the linear region are very similar with TTFA(7),

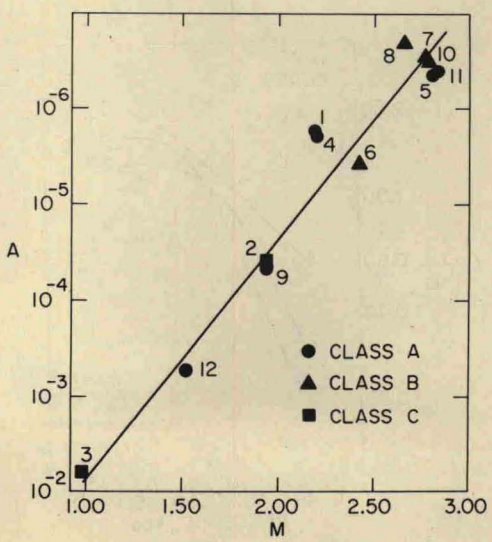

FIG. 15. Log A vs M—all compounds.

BTFA(8), and PACA(10) between 2.65 and 2.78; FTFA(6) is slightly lower at 2.42.

The two Class C compounds show somewhat different behavior. DBM(2) is linear only to about 75 kbars and becomes independent of pressure above 120 kbars. On the other hand, DPM(3) is linear to 120 kbars. The conversion continues to increase thereafter, but at a much reduced rate. The high pressure behavior of FTFA(6), with the distinct leveling above 135 kbars, is intermediate between DPM(3) and DBM(2).

It appears from the log$K$–log$P$ plots that there is a tendency for conversions to converge at high pressures. Thus derivatives with large initial conversions have small slopes and vice versa. This is demonstrated quite well in a plot of log$A$ vs M in Fig. 15.

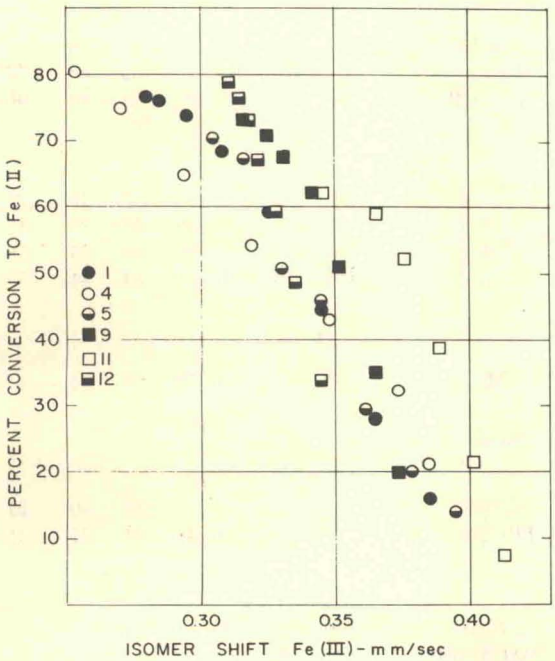

FIG. 16. Conversions vs isomer shift—Class A compounds.

All of the derivatives may be fit with a straight line. Such a correlation is noteworthy because the values of A and M cover large portions of the ranges found between ionic and covalent systems. As shown earlier, the electron donor ability decreases in the order [DPM(3), MACA(9), PACA(10), EACA(12)]> [ACA(1), DBM(2), BA(4)]>[TFACA(5), FTFA(6), TTFA(7), BTFA(8), NACA(11)] where the members of each general group have been arbitrarily arranged in order of their reference codes. Good electron donating groups, with the exception of PACA(10), tend to have large A and small M values; electron donors of intermediate strength have intermediate A and M parameters; and poor electron donors have small A and large M values.

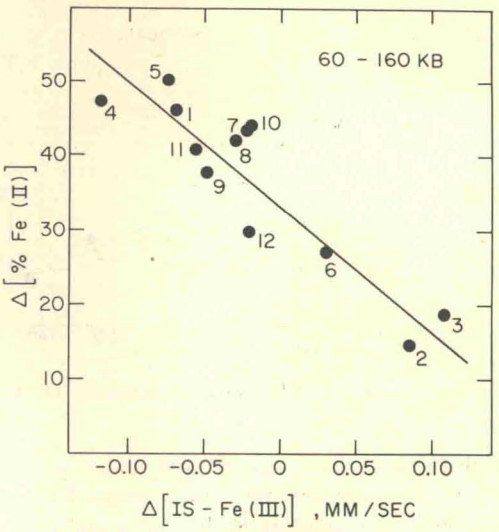

FIG. 17. Δ Conversion vs -isomer shift 60 to 160 kbars.

To the extent that the absolute value of the ferric isomer shift is a measure of the tendency of the ligand to enhance thermal electron transfer, it should be possible to correlate the Fe(III) isomer shifts and the extent of conversion to Fe(II). Class A derivatives, which are characterized as generally poor π acceptors with a range of σ donor properties, are plotted in this form of correlation in Fig. 16. There is some scatter but it is clear that, for this group of compounds, a high isomer shift (low electron density) may be associated with a small conversion and a low isomer shift (high electron density) with a high conversion. The derivative which deviates most from the rest of the compounds, NACA(11), typically shows dissimilar behavior in all of its Mössbauer parameters, perhaps due to resonance effects associated with the nitro group.

There is a reasonable correlation between isomer shift and conversion for the Class A compounds. However, as can be seen from Fig. 17, there is an excellent correlation for all twelve compounds for the *change* of

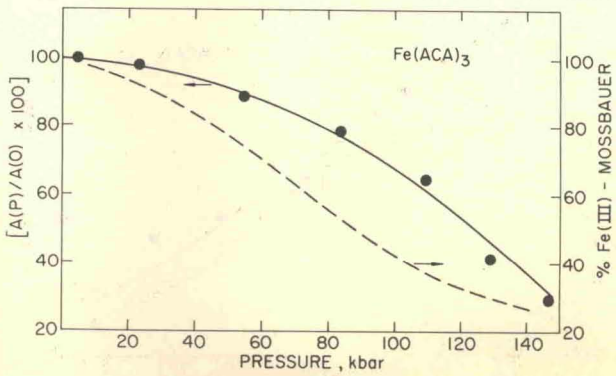

FIG. 18. Relative area under CT_1 peak vs pressure—ACA(1).

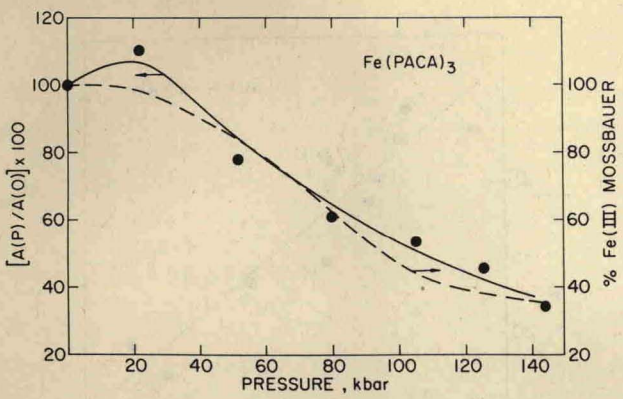

FIG. 19. Relative area under CT_1 peak vs pressure—TFACA(5).

isomer shift over the range 60–160 kbars vs the *increase* in conversion over the same range. The isomer shift depends, as discussed earlier, on a complex mixture of σ and π overlap. The conversion depends only on the location of the ligand π orbitals vis a vis the metal d_π orbitals. While the change in isomer shift with pressure contains both σ and π elements, it is apparent that the *relative* values of the change measure quite accurately the *relative* increase in availability (among the compounds) of the ligand π electrons, as the pressure increases.

Optical Spectra

Much consideration has been given to the assignment of the peaks (or band centers) of the ligand anions[34–36] and of their iron chelates.[37–48] The situation can best be explained by reference to the observed peaks in ferric acetylacetonate. There is general agreement that the high energy peaks at 235 and 272 mμ are intraligand ($\pi\rightarrow\pi^*$) transitions. There are two bands of slightly lower, but still high, intensity ($\log\epsilon\sim$ 3.5) at 351 mμ and 431 mμ. These are almost certainly associated with charge transfer as they do not appear in the ligand spectrum. A number of authors[41,42,44–46,48] have assigned the higher energy peak to metal to ligand ($t_{2g}\rightarrow\pi_4^*$) electron transfer possibly with some admixture of $\pi\rightarrow\pi^*$ character.

The second charge transfer peak at 431 mμ is the only one which has aroused appreciable controversy. Barnum[39,40] noted that $n\rightarrow t_{2g}$ and $n\rightarrow e_g$ as well as four $\pi_3\rightarrow t_{2g}$ transitions were possible but did not make any assignment; in fact, he assumed the $\pi_3\rightarrow t_{2g}$ transitions were forbidden. Murakami and Nakamura[41] assigned the 431 mμ peak to an $n\rightarrow e_g$ transition from the oxygen nonbonding electrons. This was concurred with by Singh and Sahai[42] but Lintvedt and Kernitsky,[48] while agreeing that it was a reasonable assignment, concluded that the ground state should contain both oxygen nonbonding and π components. Hanazaki, *et al.*[45,46] on the other hand, assigned the 431 mμ peak predominantly to $t_{2g}\rightarrow\pi_4^*$ character with a small amount of admixed locally excited triplet configuration. Grobelny *et al.*[44] also attribute $t_{2g}\rightarrow\pi_4^*$ character to the 431 mμ peak. Still one more interpretation was given by Mathews,[43] who treated two other iron chelates,

TABLE V. Relative area of optical charge transfer bands.

Derivative	Pressure (kbar) 20	40	60	80	100	120	140
A–CT_1 band							
Class A							
ACA(1)[a]	98	94	88	79	68	53	37
TFACA(5)[a]	113	104	89	75	62	49	37
MACA(9)[a]	111	108	101	91	78	60	40
Class B							
FTFA(6)[a]	111	112	100	78	57	38	20
TTFA(7)[a]	99	86	65	48	35	25	17
BTFA(8)[a]	107	93	78	63	48	33	18
PACA(10)[b]	107	94	78	65	53	44	37
Class C							
DPM(3)[a]	108	102	90	79	68	56	45
B–CT_2 band							
Class A							
ACA(1)[c]	100	98	92	77	58	40	21
TFACA(5)[c]	99	84	63	44	31	22	(16)
Class B							
BTFA(8)[a]	109	105	86	64	(41)		
PACA(10)[c]	101	92	82	72	(62)		
Class C							
DPM(3)[a]	111	82	48	14			

[a] Normalized at 4 kbar.
[b] Normalized at 1 atm.
[c] Normalized at 22 kbar.

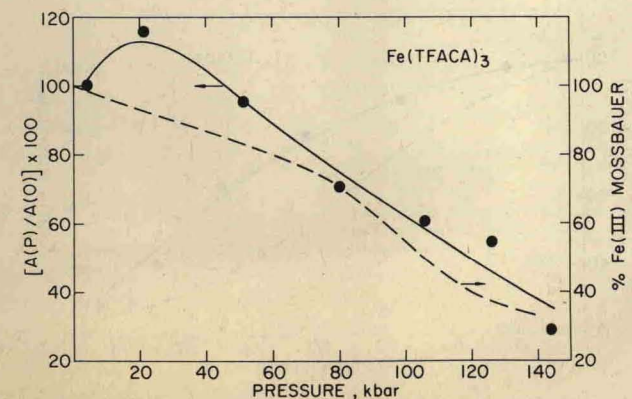

FIG. 20. Relative area under CT_1 peak vs pressure—PACA(10).

TABLE VI. Shift of $\pi \rightarrow \pi^*$ peak ($\Delta\nu$, cm^{-1}). Shift of lower energy edge (0.90 relative absorbance). Pressure (kbar).

Derivative	ν_0	20	40	60	80	100	120	140
				Class A				
ACA(1)	34 610	−200	−425	−670	−925	−1185	−1500	−1970
TFACA(5)	33 680	−70	−150	−285	−450	−665	−950	−1310
MACA(9)	33 770	−150	−250	−370	−400	−630	−760	−890
				Class B				
FTFA(6)	28 475	−270	−545	−815	−1090	(−1370)	(−1645)	
TTFA(7)	28 040	−320	−710	−915	−1220	−1530	(−1835)	
BTFA(8)	30 810	−545	−1100	−1660	−2220	(−2775)	(−3330)	
PACA(10)	33 365	−100	−220	−365	−555	−790	−1080	−1455
				Class C				
DPM(3)	34 685	−165	−345	−515	−685	−860	−1030	(−1205)

Shift of lower energy edge (0.50 relative absorbance). Pressure (kbar).

Derivative	ν_0	20	40	60	80	100	120	140
				Class A				
ACA(1)	33 120	−310	−570	−890	−1270	−1710	−2270	−3230
TFACA(5)	31 940	−240	−440	−710	−1050	−1460	−1950	−2520
MACA(9)	31 610	−220	−400	−640	−900	−1190	−1510	−1860
				Class B				
FTFA(6)	26 985	−350	−700	−1050	−1400	(−1650)		
BTFA(8)	28 425	−670	−1330	−1990	−2650	(−3310)		
PACA(10)	32 000	−360	−650	−1040	−1500	−2000	−2550	−3220
				Class C				
DPM(3)	32 820	−380	−1140	−1560	−1730	−1860	−2130	−2810

$Fe(TTFA)_3$ and $Fe(DBM)_3$, and assigned the low energy bands to various crystal field transitions. Intensity considerations would seem to rule out this possibility however.

Neither of the peaks can be directly associated with the $\pi_3 \rightarrow t_{2g}$ transfer presumably involved in the reduction. In any case, however, the areas under the charge transfer peaks should correlate approximately with the fraction of ferric sites present.

The areas of the two charge transfer bands in the high pressure optical spectra have been estimated by assuming Gaussian shapes and subtracting the large tail of the intense intraligand transition. The two charge transfer bands were treated independently; hence the "background" subtracted involves both the $\pi \rightarrow \pi^*$ tail and a portion of the other charge transfer band. Thus the absolute values of the bandwidths and intensities may be incorrect but the trends in the area changes are considered a good first order approximation.

TABLE VII. Shift of CT_1 band center ($\Delta\nu$, cm^{-1}). Pressure (kbar).

Derivative	ν_0	20	40	60	80	100	120	140
				Class A				
ACA(1)	22 190	−656	−865	−1080	−1275	−1505	−1835	−2340
TFACA(5)	22 390	−425	−550	−640	−790	−940	−1130	−1445
MACA(9)	20 550	−180	−365	−555	−740	−925	−1115	−1300
				Class B				
FTFA(6)	19 230	−300	−600	−900	−1205	−1505	−1805	−2100
TTFA(7)	20 010	−365	−700	−1035	−1355	−1700	−2140	−2750
BTFA(8)	20 440	−305	−605	−910	−1215	−1520	−1825	−2130
PACA(10)	21 300	−420	−840	−1260	−1685	−2110	−2535	−2960
				Class C				
DPM(3)	22 975	−215	−430	−635	−830	−1070	−1365	−1775

TABLE VIII. Shift of CT_2 band center ($\Delta\nu$, cm^{-1}). Pressure (kbar).

Derivative	ν_0	20	40	60	80	100	120	140
				Class A				
ACA(1)	28 405	−140	−270	−410	−550	−690	−830	(−960)
TFACA(5)	27 425	−150	−290	−340	−590	−735	−880	(−1025)
MACA(9)	26 600			−850	−850			
				Class B				
FTFA(6)	25 320	−130	−260	−385	(−520)	(−650)		
BTFA(8)	25 520	−295	−590	−835	(−1180)	(−1470)		
PACA(10)	26 985	−80	−180	−340	−620	(−1000)		
				Class C				
DPM(3)	28 170	−230	−460	−695	−925	(−1155)		

Figures 18, 19, and 20 show the normalized area of the lower energy charge transfer band CT_1 as a function of pressure for ACA(1), TFACA(5), and PACA(10). The smoothed area estimates for both charge transfer bands of these and the remaining derivatives for which optical data were obtained are included in Table V. The data points and the solid curve refer to the normalized area; the dashed curve represents the percent of ferric ion as obtained from Mössbauer measurements. As seen in these typical examples, the charge transfer band area estimations generally fall somewhat above the Mössbauer ferric ion concentration curve. This is not unreasonable since previous high pressure optical measurements by Stephens and Drickamer[49] showed a general increase in charge transfer band intensity with pressure in several inorganic and organic complexes. This indicates an increase in transition moment with decreasing interatomic distance and is consistent with Mulliken's[50,51] theoretical work on charge transfer spectra. Thus there is competition between the increase in intensity expected because of the charge transfer character and the decrease accompanying the loss of ferric sites as they are converted to ferrous sites. Nevertheless, the agreement is very good (in some cases it is probably fortuitous). This has important implications in the examination of high pressure changes of oxidation state in other transition metal complexes which cannot be measured with Mössbauer resonance.

In addition to the estimation of the charge transfer band areas, measurements of the positions and shifts of all absorption peaks were made. These latter data are not essential for this study but are included as they may be useful in other work. The positions of the charge transfer band centers (CT_1 and CT_2) may be correlated with the intraligand $\pi\rightarrow\pi^*$ transition as shown in Fig. 21. The data were obtained from KBr spectra at atmospheric pressure. Such a correlation may arise from admixing of locally excited ligand functions or from coincidence of ground or excited states. The red shifts of all absorption peaks to lower energy with increasing pressure are given in Tables VI, VII, and VIII. No general correlation between the shifts of the charge transfer peaks and the intraligand transition peak was observed. The intraligand band shows appreciable broadening with increasing pressure, as has also been observed by Fisher and Drickamer[5] and Grenoble *et al.*[7] The broadening was less extreme for the charge transfer bands. The high pressure data allow brief comment on the possible assignments, of which only the lower energy charge transfer band is in question. Calculation of the effect of pressure on the crystal field splitting based on Lintvedt's[49] assignments (i.e., CT_1 is $\pi\rightarrow e_g$, CT_2 is $t_{2g}\rightarrow\pi^*$) does not yield reasonable trends in the e_g–t_{2g} energy difference. Some derivatives show small initial increases; however, in general decreases of the order of 1000 cm^{-1} are observed at 100 kbars. All other high spin systems studied in this laboratory have shown increases of this same order in the ligand field splitting. This, plus the fact that no peak appears in the near infrared corresponding to a $\pi\rightarrow t_{2g}$ transition casts considerable doubt on Lintvedt's assignments. It may also be that there is significant $\pi\rightarrow\pi^*$ admixture in these peaks as suggested by Hanazaki *et al.*[46,47] although the intensity changes with pressure assure the predominant charge transfer character.

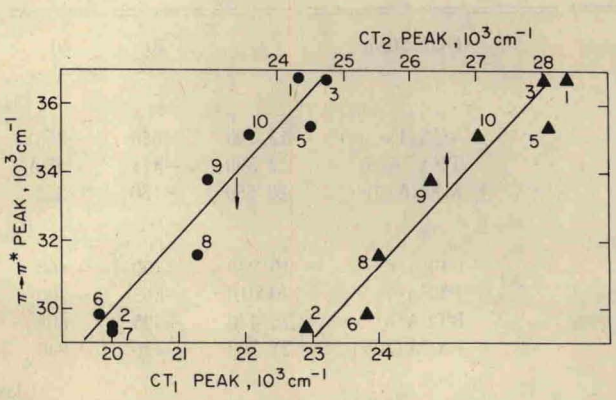

FIG. 21. Location of intraligand vs charge transfer peaks—atmospheric pressure.

APPENDIX

Quadrupole Splitting

The behavior of the ferric and ferrous quadrupole splittings was also examined as a function of pressure. Since the ferric ion has a spherically symmetric *d* electron shell, its quadrupole splitting is initially rather small. Changes with pressure reflect predominantly the changes in electric field gradient because of local deviations from cubic (octahedral) symmetry. Changes in the ferrous quadrupole splitting are more difficult to analyze since the occupation of the asymmetric *d* electron shell is the primary factor (leading to the large initial quadrupole splitting) and the effect of pressure on this factor is less well-defined. There is a general tendency for the ferric quadrupole splitting to increase over the pressure range (see Table II). For clarity of presentation, the 12 derivatives have been divided into two groups according to structural considerations, rather than the three classes based on electronic factors. Group I consists of the asymmetrically substituted chelates BTFA(8), FTFA(6), TTFA(7), BA(4), and TFACA(5) which are listed in decreasing order of their quadrupole splittings at the highest pressures. Group II consists of the symmetrically substituted derivatives DBM(2), NACA(11), ACA(1), EACA(12), DPM(3), MACA(9), and PACA(10), also listed in decreasing order. At low pressures there is no distinction between the groups with the quadrupole splittings for all the derivatives lying between 0.63–0.91 mm/sec at 20 kbars. As the pressure increases there is a definite tendency for the asymmetric derivatives (Group I) to exhibit larger quadrupole splittings although there is measurable overlap of the groups even at the highest pressures. The high pressure range of Group I is 1.60–1.85 mm/sec; Group II falls in the region 1.42–1.68 mm/sec. Thus the electric field gradient must increase slightly more for the asymmetrically substituted derivatives than for the symmetrically substituted ones.

There was no obvious classification of the ferrous quadrupole splittings into smaller subgroups, either on structural or electronic grounds. Although the ferrous quadrupole splittings generally show more scatter than the ferric values, it is still possible to establish a range of 2.0–2.5 mm/sec at 20 kbars and a general decrease in splitting of the order of 0.1 mm/sec over the pressure range. In many compounds it appears that the data go through shallow minima between 80–120 kbars.

* This work was supported in part by the U.S. Atomic Energy Commission under Contract AT(11-1)-1198.

[1] P. de Brunner, R. W. Vaughan, A. R. Champion, J. Cohen, J. Moyzis, and H. G. Drickamer, Rev. Sci. Instr. **37,** 1310 (1966).
[2] R. A. Fitch, T. E. Slykhouse, and H. G. Drickamer, J. Opt. Soc. Am. **47,** 1015 (1957).
[3] H. G. Drickamer and A. S. Balchan, in *Modern Very High Pressure Techniques*, edited by R. H. Wentorf, Jr. (Butterworths, London, 1962).
[4] H. G. Drickamer, V. C. Bastron, D. C. Fisher, and D. C. Grenoble, Solid State Chem. **2,** 94 (1970). (This paper contains references to papers published before 1970.)
[5] D. C. Fisher and H. G. Drickamer, J. Chem. Phys. **54,** 4825 (1971).
[6] D. C. Grenoble and H. G. Drickamer, J. Chem. Phys. **55,** 1624 (1971).
[7] D. C. Grenoble, C. W. Frank, C. B. Bargeron, and H. G. Drickamer, J. Chem. Phys. **55,** 1633 (1971).
[8] C. B. Bargeron, M. Avinor, and H. G. Drickamer, Inorg. Chem. **16,** 1338 (1971).
[9] C. B. Bargeron and H. G. Drickamer, J. Chem. Phys. **55,** 3471 (1971).
[10] C. P. Slichter and H. G. Drickamer, J. Chem. Phys. (to be published).
[11] R. A. Marcus, Ann. Rev. Phys. Chem. **15,** 155 (1964).
[12] R. A. Marcus, J. Chem. Phys. **43,** 1261 (1965).
[13] N. S. Hush, *Progress in Inorganic Chemistry* **8,** 357, edited by F. A. Cotton (Interscience, New York, 1967).
[14] N. S. Hush, Electrochim. Acta **13,** 1005 (1968).
[15] A. Hantzsch and C. H. Desch, Annalen **323,** 1 (1902).
[16] D. N. Sen and N. Thankarajan, Indian J. Chem. **3,** 215 (1965).
[17] J. W. G. Wignall, J. Chem. Phys. **44,** 2462 (1966).
[18] H. C. Brown and Y. Okamoto, J. Am. Chem. Soc. **80,** 4979 (1958).
[19] S. M. Schildcrout, R. G. Pearson, and F. E. Stafford, J. Am. Chem. Soc. **90,** 4006 (1968).
[20] G. M. Bancroft, C. Reichert, and J. B. Westmore, Inorg. Chem. **7,** 870 (1968).
[21] G. M. Bancroft, C. Reichert, J. B. Westmore, and H. D. Gessor, Inorg. Chem. **8,** 474 (1969).
[22] C. Reichert and J. B. Westmore, Inorg. Chem. **8,** 1012 (1969).
[23] C. Reichert, G. M. Bancroft, and J. B. Westmore, Can. J. Chem. **48,** 1362 (1970).
[24] C. Reichert and J. B. Westmore, Can. J. Chem. **48,** 3213 (1970).
[25] H. F. Holtzclaw, Jr., R. L. Lintvedt, H. E. Baumgarter, R. G. Parker, M. M. Bursey, and P. F. Rogerson, J. Am. Chem. Soc. **91,** 3774 (1969).
[26] H. F. Holtzclaw, Jr., K. W. R. Johnson, and F. G. Hengeveld, J. Am. Chem. Soc. **74,** 3776 (1952).
[27] H. F. Holtzclaw, Jr., A. H. Carlson, and J. P. Collman, J. Am. Chem. Soc. **78,** 1838 (1956).
[28] E. R. Nightingale, Jr., and H. F. Holtzclaw, Jr., J. Am. Chem. Soc. **81,** 3523 (1959).
[29] R. L. Lintvedt, H. D. Russell, and H. F. Holtzclaw, Jr., Inorg. Chem. **5,** 1603 (1966).
[30] N. E. Erickson, in *Mössbauer Effect and Its Chemical Applications*, edited by P. F. Gould (American Chemical Society, Washington, 1967).
[31] H. G. Drickamer and J. C. Zahner, Advan. Chem. Phys. **4,** 161 (1962).
[32] H. G. Drickamer in *Solid State Physics*, edited by F. Seitz and D. Turnbull (Academic, New York, 1965), Vol. 17, p. 1.
[33] S. C. Fung and H. G. Drickamer, J. Chem. Phys. **51,** 4353 (1969).
[34] R. L. Belford, A. E. Martell, and M. Calvin, J. Inorg. and Nucl. Chem. **2,** 11 (1956).
[35] F. Hashimoto, J. Tanaka, and S. Nagakura, J. Mol. Spectry. **10,** 401 (1963).
[36] L. S. Forster, J. Am. Chem. Soc. **86,** 3001 (1964).
[37] R. H. Holm and F. A. Cotton, J. Am. Chem. Soc. **80,** 5658 (1958).
[38] D. W. Barnum, J. Inorg. and Nucl. Chem. **21,** 221 (1961).
[39] D. W. Barnum, J. Inorg. and Nucl. Chem. **22,** 183 (1961).
[40] C. K. Jorgensen, Acta Chem. Scand. **16,** 2406 (1962).
[41] Y. Murakami and K. Nakamura, Bull. Chem. Soc. Japan **39,** 901 (1966).
[42] R. R. Singh and R. Sahai, Australian J. Chem. **22,** 1169 (1969).
[43] C. K. Mathews, J. Inorg. and Nucl. Chem. **31,** 2853 (1969).
[44] R. Grobelny, B. Jezowska-Trzebiatoswka, and W. Wojciechowski, Bull. Acad. Polon. Sci. **17,** 285 (1969).
[45] I. Hanazaki, F. Hanazaki, and S. Nagakura, J. Chem. Phys. **50,** 265 (1969).
[46] I. Hanazaki, F. Hanazaki, and S. Nagakura, J. Chem. Phys. **50,** 276 (1969).
[47] E. A. Magnuson, R. A. Thomson, and A. G. Wedd, Chem. Commun. 842 (1969).
[48] R. L. Lintvedt and L. K. Kernitsky, Inorg. Chem. **9,** 491 (1970).
[49] D. R. Stephens and H. G. Drickamer, J. Chem. Phys. **30,** 1518 (1959).
[50] R. S. Mulliken, J. Am. Chem. Soc. **74,** 811 (1952).
[51] R. S. Mulliken, J. Phys. Chem. **56,** 801 (1952).